Pattern formation in flows of asymmetrically interacting particles: Peristaltic pedestrian dynamics as a case study

Gaididei, Yuri B.; Marschler, Christian; Sørensen, Mads Peter; Christiansen, Peter L.; Rasmussen, Jens Juul

Published in:
Evolution Equations and Control Theory

Link to article, DOI:
10.3934/eect.2019005

Publication date:
2019

Document Version
Peer reviewed version

EVOLUTION EQUATIONS AND
CONTROL THEORY
Volume **8**, Number **1**, March **2019**

doi:10.3934/eect.2019005

pp. **X–XX**

PATTERN FORMATION IN FLOWS OF ASYMMETRICALLY INTERACTING PARTICLES: PERISTALTIC PEDESTRIAN DYNAMICS AS A CASE STUDY

Yuri B. Gaididei

Bogolyubov Institute for Theoretical Physics
Metrologichna str. 14B
01413 Kiev, Ukraine

Christian Marschler

Continental AG, Vahrenwalder Strasse 9
D-30165 Hanover, Germany

Mads Peter Sørensen*

Department of Applied Mathematics and Computer Science
Technical University of Denmark
DK-2800 Kongens Lyngby, Denmark

Peter L. Christiansen

Department of Physics and Department of Applied Mathematics and Computer Science
Technical University of Denmark
DK-2800 Kongens Lyngby, Denmark

Jens Juul Rasmussen

Department of Physics, Technical University of Denmark
DK-2800 Kongens Lyngby, Denmark

Jens Starke

Institute of Mathematics, University of Rostock
D-18057 Rostock, Germany

Abstract. The influence of asymmetry in the coupling between repulsive particles is studied. A prominent example is the social force model for pedestrian dynamics in a long corridor where the asymmetry leads to anisotropy in the repulsion such that pedestrians in front, i.e., in walking direction, have a bigger influence on the pedestrian behavior than those behind. In addition to one- and

2000 *Mathematics Subject Classification.* Primary: 37N20, 37K60, 37M05, 70K50; Secondary: 70H09, 70K60, 70K75.

Key words and phrases. Nonlinear lattice dynamics, pedestrian flow, pattern formation in complex systems, asymmetry, general perturbation schemes, bifurcations and instability, and nonlinear modes.

This work is supported by Civilingeniør Frederik Leth Christiansens Almennyttige Fond, the Otto Mønsteds Fond and a special program of the National Academy of Sciences of Ukraine.

* Corresponding author: Mads Peter Sørensen.

two-lane free flow situations, a new traveling regime is found that is reminiscent of peristaltic motion. We study the regimes and their respective stability both analytically and numerically. First, we introduce a modified social force model and compute the boundaries between different regimes analytically by a perturbation analysis of the one-lane and two-lane flow. Afterwards, the results are verified by direct numerical simulations in the parameter plane of pedestrian density and repulsion strength from the walls.

1. **Introduction.** The understanding of pedestrian dynamics is critical for both researchers and managers. It is crucial in designing various public facilities such as railway stations, airports, supermarkets, etc. Pedestrian flow dynamics can be considered as a particular example of collective non-equilibrium behavior of asymmetrically nonlinearly coupled elements [10, 11, 2, 30]. Many collective phenomena such as non-equilibrium phase transitions, pattern formations and bifurcations are inherent features of such models. Examples are traffic flow on single lane highways and road networks [10, 18, 31]; and flows through bottlenecks where pedestrians spontaneously form several trails [14, 27].

Two approaches are commonly used in microscopic modeling of pedestrian dynamics: discrete and continuous ones. In the discrete approach the motion of pedestrians is considered discrete in time and space in terms of cellular automata (see e.g., [3]). By modeling long-range interactions between the pedestrians by a so-called "floor field", which modifies the transition rates to neighbouring cells, a spontaneous emergence of lanes in counterflow through a large corridor in the framework of the automaton model was demonstrated in [4]. The continuous approach describes the microscopic pedestrian dynamics in terms of time- and space-continuous ordinary differential equations. The collective character of pedestrian flow is due to person-person interaction originating from a person's desire to avoid colliding with other pedestrians and also to prevent collisions with walls and obstacles. One of the most popular microscopic models is the social-force model introduced in [12] and further-developed in numerous studies (see e.g. the review paper [16]). In the framework of this approach, a crowd of pedestrians is modeled as an ensemble of mass points moving in a two-dimensional domain. The pedestrian dynamics is encoded in the form of differential Newton-like equations of motion of particles, which move in some potential profile (it models the presence of walls and obstacles) under the influence of inter-particle interaction forces (social forces). Within this model, bidirectional flows of pedestrians are studied where spontaneous formation of lanes consisting of pedestrians with a uniform walking direction and oscillatory changes of the walking direction at narrow passages were analysed [12] and different types of patterns, e.g., jams, strip formation, and turbulent waves, were reported [13, 32, 16].

Quite recently we investigated pattern formation in a annular channels for repulsive interaction with finite range [21]. Due to complicated geometry and type of particle interactions this study was based on numerical investigations. Therefore, in the present study we investigate a simpler model for particles moving in a straight corridor with exponential-like inter-particle interactions and parabolic interactions with the walls. This allows us to study this problem both analytically and numerically and clarify mechanisms, which control the pattern formation. We consider the pedestrian flow in the framework of the continuous social-force model [12, 13], but in contrast to the original model we include the fact that the social force can be asymmetric: an interaction with a neighbor ahead differs from the interaction with

the neighbor behind. In other words, we consider the pedestrian flow as a dynamical system of *asymmetrically interacting* particles. We show that the pedestrian dynamics depends strongly on the density of the crowd, on the strength of the inter-person interaction and interaction with walls, as well as on the degree of the social force asymmetry. When the social force is symmetric the pedestrian flow may be either single- or multi-lane. The transition between these two regimes is similar to a topological zig-zag phase transition, which involves a quasi-one-dimensional chain of interacting particles confined in a narrow channel [28, 9, 7, 20]. In the case of short-ranged interparticle interaction there is area of parameters where phases coexist and hysteretic behavior takes place [6]. When the asymmetry of the social interaction is taken into account a new pattern of moving "bubbles" arises when the distance between lanes becomes spatially modulated and changes periodically in time, i.e., a pattern resembling a peristaltic motion. We find the transition from the zig-zag state to the peristaltic state to be characterized by a Hopf bifurcation (either sub- or supercritical) [25]. All transitions are determined analytically and later on verified by direct numerical simulations, which are in perfect agreement with the transition curves from our theoretical studies.

This paper is organized as follows. In Section 2, we present the model. In Section 3, the results of the stability analysis and numerics for the free-flow solution are presented. Stability and dynamics of the one-lane flow are discussed in Section 4. Numerical results relating to the existence and stability of peristaltic solutions are discussed in Section 5. In Section 6 localized states and their dynamics are studied in the frame of collective coordinate approach. Section 7 describes the limiting case of the dynamics in the continuum limit. Finally, Section 8 contains some concluding remarks and an outlook on future research directions.

2. Particle model with asymmetric interactions.

We consider the dynamics of N pedestrians, who move along a corridor. In the spirit of the social force model [12, 13] we assume that each pedestrian likes to move with a certain preferred velocity $\boldsymbol{v}$ and tries to avoid collisions with other pedestrians and the corridor walls. The equation of motion for the n-th pedestrian, $n = 1, \ldots, N$, has the form

$$\frac{d\boldsymbol{r}_n}{dt} = \boldsymbol{v} + \boldsymbol{f}_n - \frac{\partial V_w(\boldsymbol{r}_n)}{\partial \boldsymbol{r}_n}, \tag{1}$$

where $\boldsymbol{r}_n = (x_n, y_n)$ is the position of the n-th pedestrian. The first term on the right-hand side represents an intention of the pedestrian to move with a velocity $\boldsymbol{v}$, $\boldsymbol{f}_n$ represents a force with which the n-th person is repelled from other pedestrians and V_w is a potential modeling the wall interaction. It is feasible that the "interaction force" between pedestrians is asymmetric [8]: usually we pay different attention to neighbors who are in front of us than behind of us. It appears natural to define the notion "forward-backward" with respect to the walking direction defined by the unit vector $\boldsymbol{e_v} = \frac{\boldsymbol{v}}{v}$ and write the interaction force $\boldsymbol{f}_n$ in the form

$$\boldsymbol{f}_n = -\frac{\partial V}{\partial \boldsymbol{r}_n} + \epsilon \left| \boldsymbol{e_v} \cdot \frac{\partial V}{\partial \boldsymbol{r}_n} \right| \boldsymbol{e_v} \,. \tag{2}$$

Here, V is a repulsive interaction potential which we choose as

$$V = \frac{A}{2\alpha} \sum_{\substack{n,m \\ (n \neq m)}} \exp(-\alpha \mid \boldsymbol{r}_n - \boldsymbol{r}_m \mid), \tag{3}$$

where the constants A and α characterize, respectively, the intensity and inverse range of the inter-pedestrian interaction. The parameter ϵ characterizes the strength of the asymmetry of the interaction. The last term on the right-hand side of Eq. (1) represents an interaction with corridor walls. We study pedestrian dynamics in a long narrow corridor aligned along the x-axis. We assume that the most preferable position for a pedestrian is the corridor midline ($y = 0$) and for this interaction with the corridor walls we use a parabolic potential

$$V_w(\boldsymbol{r}) = \frac{1}{2}\nu y^2 \,, \tag{4}$$

with a constant ν characterizing the strength of the interaction. The desired velocity $\boldsymbol{v}$ is assumed to be parallel to the x-axis, i.e., $\boldsymbol{v} = (v, 0)^T$. Thus, Eq. (1) presented in its two spatial components takes the form

$$\begin{aligned} \frac{d}{dt}x_n &= A\sum_{l\neq 0}\left(1+\epsilon\,\frac{l}{|l|}\right)(x_n - x_{n+l})\,F\Big(|\boldsymbol{r}_{n+l}-\boldsymbol{r}_n|\Big) + v, \\ \frac{d}{dt}y_n &= A\sum_{l\neq 0}(y_n - y_{n+l})\,F\Big(|\boldsymbol{r}_{n+l}-\boldsymbol{r}_n|\Big) - \nu\, y_n \,, \end{aligned} \tag{5}$$

where $l \in \{-J, \ldots, -1, +1, \ldots, J\}$ with J being the number of neighbors which are taken into account for interactions and

$$F(r) = \frac{e^{-\alpha r}}{r} \,. \tag{6}$$

We study the pedestrian dynamics with periodic boundary conditions

$$x_{n+N} = x_n + L, \quad y_{n+N} = y_n \tag{7}$$

for the positions (x_n, y_n) of N pedestrians in a corridor of length L.

To simplify the notation it is convenient to rescale the variables as follows

$$\begin{aligned} (\bar{x}_n, \bar{y}_n) &= \alpha(x_n, y_n) \,, \quad \bar{t} = A\alpha\, t, \\ \bar{\nu} &= \frac{\nu}{A\alpha}, \quad \bar{v} = \frac{v}{A} \,. \end{aligned} \tag{8}$$

In terms of the new variables the equations of motion (5) can be written as

$$\frac{d}{d\bar{t}}\bar{x}_n = \sum_{l\neq 0}\left(1+\epsilon\,\frac{l}{|l|}\right)\frac{(\bar{x}_n - \bar{x}_{n+l})}{|\bar{\boldsymbol{r}}_{n+l}-\bar{\boldsymbol{r}}_n|}\,\exp\Big(-|\bar{\boldsymbol{r}}_{n+l}-\bar{\boldsymbol{r}}_n|\Big) + \bar{v}, \tag{9a}$$

$$\frac{d}{d\bar{t}}\bar{y}_n = \sum_{l\neq 0}\frac{(\bar{y}_n - \bar{y}_{n+l})}{|\bar{\boldsymbol{r}}_{n+l}-\bar{\boldsymbol{r}}_n|}\,\exp\Big(-|\bar{\boldsymbol{r}}_{n+l}-\bar{\boldsymbol{r}}_n|\Big) - \bar{\nu}\,\bar{y}_n \,. \tag{9b}$$

Equations (9) show that without loss of generality we can confine ourselves to the case when $A = \alpha = 1$. Therefore in what follows we restrict ourselves to this case and study the pedestrian dynamics by using Eqs. (9) omitting the 'bar' notations.

3. **Stationary free flow solutions.** Equations (9) have explicit solutions which we refer to as the free flow solutions as they correspond to the situation in which all pedestrians move with the same constant velocity and equal spacing between neighbors. There are two types of these free flow solutions (see Fig. 1 obtained by direct numerical solutions of Eqs. (9)).

One-lane flow: all pedestrians move in a single line with the same velocity c_1 and keep the same distance $a = 1/\rho = L/N$ between them (see Fig. 1(a)), i.e.,

$$x_n = na + c_1 t, \quad y_n = 0, \tag{10}$$

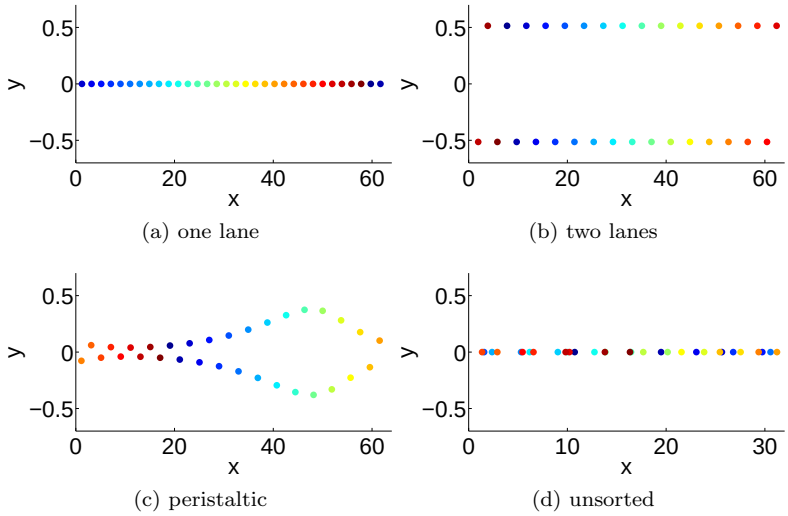

FIGURE 1. Patterns emerging in the pedestrian model. Color indicates pedestrian index. Numerical solution of Eqs. (9) for parameters specified in the text.

where

$$c_1 = v - 2\,\epsilon\, a \sum_{l=1}^{J} l F(la)\ . \tag{11}$$

Two-lane (zig-zag) flow: all pedestrians move in two lanes with the same velocity c_2 and keep the same distance between them (see Fig. 1(b)), i.e.,

$$x_n = na + c_2 t, \quad y_n = (-1)^n \frac{b}{2}\ , \tag{12}$$

where b is the distance between lanes, and c_2 is a common stationary velocity of the particles. By inserting Eq. (12) into Eq. (9a), we obtain that the stationary velocity c_2 is determined by the equation

$$c_2 = v - 2\epsilon a \sum_{l=1}^{J} l F(\delta_l)\ , \tag{13}$$

where

$$\delta_l = \sqrt{l^2 a^2 + \frac{b^2}{4}\left(1 - (-1)^l\right)^2} \tag{14}$$

is the distance between the n-th and $(n+l)$-th pedestrian. To find the stationary distance b between lanes we insert Eq. (12) into Eq. (9b) and obtain the equation

$$2\sum_{l=1}^{J}\left(1 - (-1)^l\right) F(\delta_l) - \nu = 0\ . \tag{15}$$

By taking into account the nearest- and next-nearest neighbor interactions (i.e., $J = 2$) and using the social force $F(r)$ in the form given by Eq. (6), we obtain that

the stationary distance b is determined by the equation

$$4\,\frac{e^{-\sqrt{a^2+b^2}}}{\sqrt{a^2+b^2}} = \nu\,. \tag{16}$$

By using the Lambert function $W(z)$, which gives the solution for W in $z = We^W$, from Eq. (16) we get

$$b = \sqrt{W^2\Big(4/\nu\Big) - a^2}\,. \tag{17}$$

As it is seen from Eq. (17) the two-lane solution exists when

$$W\Big(4/\nu\Big) \;\geq\; a \tag{18}$$

or equivalently, when

$$\nu \;\leq\; 4\,\frac{e^{-a}}{a}\,. \tag{19}$$

The function b from Eq. (17) and its comparison with full scale numerical simulations is presented in Fig. 2. The left panel of Fig. 2 displays the transverse stationary distance for a given strength of the pedestrian-wall interaction ν as a function of the pedestrian density $\rho = 1/a$. The right panel shows the distance b as a function of the pedestrian-wall interaction ν for a fixed value of pedestrian density ρ.

Note that spontaneous transition from one-lane to multi-lane pedestrian flows in corridors was experimentally observed in Ref. [14, 27, 29] (from two to five depending on the width of the corridor). The multilane flow emerges when the width exceeds some critical value [14]. In the frame of our model the role of the width plays the strength of the interaction with walls ν: the large width corresponds to small values of ν while the weak interaction with walls may be considered as analog of the large width corridor. It is worth noticing, however, that the direct application of our theory to experiments [14],[29] is rather questionable because we consider corridors with periodic boundary conditions while in the aforementioned experiments the corridors have finite length and as it was shown in [27] the lane formation depends on the length of the corridor.

In the following sections we consider the stability and dynamics of the one-lane flow and the two-lane flow separately.

4. **Dynamics of the one-lane flow.**

4.1. **Stability of the one-lane free flow.**

The stability of the free-flow solution can be assessed by considering the linearization of the system (9) about the free flow solution.

$$\begin{pmatrix} x_n \\ y_n \end{pmatrix} = \begin{pmatrix} an + c_1 t + q_n \\ (-1)^n\, p_n \end{pmatrix} \tag{20}$$

with the conditions $|p_n| \ll 1$, $|q_n| \ll 1$ on the perturbations and

$$q_{n+N} = q_n\,, \qquad p_{n+N} = p_n \quad \forall n\,.$$

In the one-lane case (10) linear longitudinal (along the x-axis) modes and transversal (along the y-axis) modes split:

$$\frac{d}{dt}q_n = -\sum_{l=1}^{J} e^{-la}\Big((1+\epsilon)(q_n - q_{n+l}) + (1-\epsilon)(q_n - q_{n-l})\Big)\,, \tag{21}$$

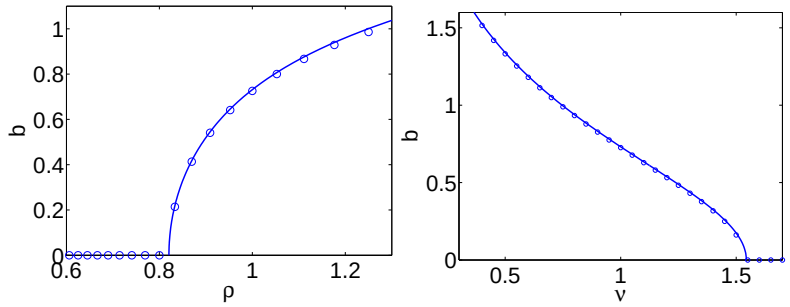

(a) $b(\rho)$ for fixed $\nu = 1$ (b) $b(\nu)$ for fixed $\rho = 1$

FIGURE 2. Transverse stationary distance b between pedestrians in the two-lane zig-zag flow shown in Fig. 1 (b). Panel (a): b vs. density ρ for fixed $\nu = 1$, panel (b): b vs. interaction strength ν for fixed $\rho = 1$, ρ being pedestrian density, ν being strength of pedestrian wall interaction. Panel (a): in the region to the left (right) of the curve the flow is single (two-) lane. Panel (b): in the region to the left (right) of the curve the flow is two- (single) lane. Direct numerical simulations (circles) and analytical predictions (curves) are in agreement.

$$\frac{d}{dt}p_n = -\nu p_n + \sum_{l=1}^{J} \frac{e^{-la}}{la}\Big[2p_n - (-1)^l\,(p_{n+l} - p_{n-l})\Big]. \tag{22}$$

The stability is analyzed by considering solutions of the linear system (21) and (22) of the form

$$\begin{aligned} q_n(t) &= \hat{q}_k\, e^{ikn}, \\ p_n(t) &= \hat{p}_k\, e^{ikn}, \end{aligned} \tag{23}$$

where

$$k = \frac{2\pi j}{N} \quad \text{with} \quad j = -\frac{N}{2} + 1, \ldots, \frac{N}{2} \tag{24}$$

is a wave number and $\hat{p}_k, \hat{q}_k$ are time-dependent amplitudes which satisfy the equations

$$\begin{aligned} \frac{d}{dt}\hat{q}_k + \Big((1+\epsilon)g_k + (1-\epsilon)g_k^*\Big)\,\hat{q}_k = 0\,, \\ \frac{d}{dt}\hat{p}_k + \Big(\nu - h_k\Big)\,\hat{p}_k = 0\,, \end{aligned} \tag{25}$$

where the notations

$$\begin{aligned} g_k &= \sum_{l=1}^{J} e^{-la}\Big(e^{ikl} - 1\Big)\,, \\ h_k &= 2\sum_{l=1}^{J} \frac{e^{-la}}{la}\Big(1 - (-1)^l\,\cos k\,l\Big) \end{aligned} \tag{26}$$

are used and * denotes complex conjugation. The solution of Eqs. (25) is given by

$$\begin{aligned} \hat{q}_k &= \tilde{q}_k e^{z_k\,t}, \\ \hat{p}_k &= \tilde{p}_k e^{z_k\,t}, \end{aligned} \tag{27}$$

where $\tilde{q}_k$ and $\tilde{p}_k$ are constant amplitudes and z_k is a complex rate. If the real part $\Re(z_k)$ of z_k is larger than zero the one-lane free flow is unstable. Insertion of Eq. (27) into Eqs. (21) and (22) leads to the two following equations for the complex frequency z_k, correspondingly,

$$z_k + (1+\epsilon)g_k + (1-\epsilon)g_k^* = 0\,, \tag{28}$$

$$z_k + \nu - h_k = 0\,. \tag{29}$$

The roots of Eq. (28) always have negative real parts and the one-lane flow (10) is stable with respect to the longitudinal modes. The roots of Eq. (29) have negative real parts and the one-lane flow (10) is stable with respect to the transversal modes when

$$\nu > \frac{2}{a}\sum_{l=1}^{J}\frac{e^{-la}}{l}\left(1-(-1)^l\right). \tag{30}$$

In the case of the next-nearest neighbor interaction ($J=2$) this inequality is reduced to

$$\nu > \frac{4}{a}\,e^{-a} \quad \text{or, equivalently, for} \quad a > W\Big(\frac{4}{\nu}\Big). \tag{31}$$

For the opposite inequality to (30) the one-lane flow is unstable with respect to the transversal mode with $k=0$ and a two-lane pattern arises.

4.2. **Dynamics of the one-lane flow.** In this subsection we consider how the system evolves to its equilibrium state in the area of parameters ρ, ν where the one-lane flow is stable, *i.e.* when the inequality given by (31) holds. We consider the case when the transversal coordinates $y_n = 0$. In this case the dynamics of the one-lane flow is described by equations

$$\frac{d}{dt}q_n = \sum_{l=1}^{J} e^{-la}\Big[-(1+\epsilon)\,e^{-(q_{n+l}-q_n)} + (1-\epsilon)\,e^{-(q_n-q_{n-l})}\Big] + \epsilon\,(v-c_1),$$

$$q_{n+N} = q_n, \quad \forall n\,, \tag{32}$$

where the periodic part of the longitudinal coordinate q_n is defined by Eq. (20). Let us first consider the case of a *totally asymmetric social interaction:* $\epsilon = 1$. By using the substitution

$$Q_n = e^{-q_n}\,, \tag{33}$$

Equation (32) reduces to a linear one

$$\frac{d}{dt}Q_n = 2\sum_{l=1}^{J} e^{-la}\,Q_{n+l} - (v-c_1)\,Q_n\,,$$

$$Q_{n+N} = Q_n, \quad \forall n\,. \tag{34}$$

Equation (34) can be easily solved, by applying the Fourier transform (23), and its solution has the form

$$Q_n(t) = \sum_{n'} K_{n-n'}(t)\,Q_{n'}(0). \tag{35}$$

Here the kernel $K_n(t)$ is given by

$$K_n(t) \equiv \frac{1}{N}\sum_k e^{ikn+2\,t\,g_k} \tag{36}$$

where the function g_k is defined by Eq. (26) and is given by the equation

$$g_k = \Big(\frac{1-e^{(ik-a)J}}{e^{a-ik}-1} - \frac{1-e^{-aJ}}{e^a-1}\Big)\,. \tag{37}$$

As an example let us consider the flow dynamics with a local initial disturbance of the form

$$q_n(0) = -\delta q\,\delta_{nn_0}, \quad \text{i.e.} \quad Q_n(0) = 1 + (e^{\delta q}-1)\,\delta_{nn_0} \tag{38}$$

In this case, as it follows from Eqs. (33) and (35) the periodic part of the longitudinal coordinates evolve as follows

$$q_n(t) = -\ln\Big(1 + (e^{\delta q}-1)\,K_{n-n_0}(t)\Big). \tag{39}$$

In the nearest-neighbor approximation ($J=1$) and in the limit $N\to\infty$ the kernel $K_n(t)$ takes the form

$$K_n(t) = \exp\{-v_1 t\}\,\frac{2^{-n}\,e^{an}\,t^{-n}}{(-n)!}\,H(-n)\,, \tag{40}$$

where $v_1 = 2\,e^{-a}$, and

$$H(n) = \begin{cases} 0, & \text{when } n\le -1 \\ 1, & \text{when } n\ge 0 \end{cases} \tag{41}$$

is a discrete Heaviside step function.

By using Stirling's asymptotic formula, in the limit $v_1\,t \sim |n-n_0| \gg 1$, $|v_1\,t + n - n_0| < v_1\,t$ the function $q_n(t)$ can be presented approximately as

$$q_n(t) = -\ln\Big(1 + (e^{\delta q}-1)\,\frac{e^{-\frac{(n-n_0+v_1\,t)^2}{2c\,t}}}{\sqrt{2\pi\sigma_1\,t}}\Big) \approx (e^{\delta q}-1)\,\frac{1}{\sqrt{2\pi v_1 t}}\,e^{-\frac{(n-n_0+v_1\,t)^2}{2\sigma_1 t}}\,. \tag{42}$$

where $\sigma_1 = v_1 = 2\,e^{-a}$. In a general case of long-range social interaction for $t\gg 1$ one can obtain approximately from Eqs. (35), (36) that

$$q_n(t) \approx (e^{\delta q}-1)\frac{1}{\sqrt{2\pi\,\sigma_J t}}\,e^{-\frac{(n-n_0+v_J\,t)^2}{2\,\sigma_J\,t}} \tag{43}$$

where

$$v_J = 2\,\frac{e^{-aJ}\left(e^{aJ+a} - e^a(J+1) + J\right)}{(e^a-1)^2}\,,$$

$$\sigma_J = 2\,\frac{e^{-aJ}\left(e^a\left(2J^2+2J-1\right) + e^{a(J+2)} + e^{aJ+a} - e^{2a}(J+1)^2 - J^2\right)}{(e^a-1)^3}\,. \tag{44}$$

The initial disturbance (38) evolves into a pulse, which propagates with the velocity v_J and preserves its self-similar shape in the coordinate frame $\Big((v_J\,t+n-n_0)/\sqrt{t}, t\Big)$. The amplitude of the pulse decreases as $t^{-1/2}$.

For *arbitrary* $\epsilon\in(0,1)$ the discrete equation (32) cannot be solved analytically. By assuming that $|q_n(t)|\ll 1$ one can expand the exponential functions in Eq. (32) and obtain Eq. (32) in the form

$$\begin{aligned}\frac{d}{dt}q_n \;=\; & \sum_{l=1}^{J}\Big[q_{n+l} + q_{n-l} - 2q_n + \epsilon\,(q_{n+l} - q_{n-l}) - \\ & \frac{1}{2}(1+\epsilon)(q_{n+l}-q_n)^2 + \frac{1}{2}(1-\epsilon)(q_{n-l}-q_n)^2\Big]\,.\end{aligned} \tag{45}$$

We extend Eq. (45) by allowing n to be a continuous variable: $q_n(t) = q(n,t)$ and by expanding the functions $q(n \pm l, t)$ into Taylor series, arrive at the Burgers equation:

$$\partial_t q = \epsilon\, v_J\, \partial_n q - \epsilon\, \frac{\sigma_J}{2} \Big(\partial_n q\Big)^2 + \frac{\sigma_J}{2}\, \partial_n^2 q\,. \tag{46}$$

The transform of Eq. (46) to a moving frame of reference: $\bar{n} = n + v_J\, t$ and usage of the Cole-Hopf transformation: $q(\bar{n}, t) = -\frac{1}{\epsilon}\, \ln\theta$, turns the nonlinear equation (46) into the ordinary diffusion equation $\frac{2}{\sigma_J}\, \partial_t \theta = \partial_{\bar{n}}^2\, \theta$. The solution of Eq. (46) under the initial condition (38) has the form

$$q(n,t) = -\frac{1}{\epsilon}\, \ln\left(1 + (e^{\epsilon\, \delta q} - 1)\, \frac{e^{-\frac{(n - n_0 + \epsilon\, v_J\, t)^2}{2\sigma_J\, t}}}{\sqrt{2\pi\sigma_J\, t}}\right). \tag{47}$$

Thus, one can conclude that the evolution of the initial disturbance (38) of the one-lane free flow as a pulse which propagates with the velocity $\epsilon\, v_J$ and preserves its self-similar shape is generic.

5. **Dynamics of the two-lane flow.**

5.1. **Stability of the two-lane free flow.** In what follows we restrict ourselves to the case of nearest and next-nearest neighbor interaction $J = 2$. Instead of the x_n, y_n coordinates it is convenient to introduce new longitudinal and transversal coordinates. We transfer Eqs. (9) to a moving frame of reference:

$$x_n(t) = c_2 t + X(n,t) \tag{48}$$

where the velocity c_2 is given by Eq. (13), and instead of the alternating function $y_n(t)$ we will use a smooth function

$$Y(n,t) = (-1)^n y_n(t). \tag{49}$$

Equations for these quantities are delay differential equations

$$\begin{aligned}\partial_t\, X(n,t) = -\frac{\delta E}{\delta X(n,t)} + \epsilon \sum_{l=1,2} \Big[\Big(X(n,t) - X(n+l,t)\Big) F\Big(r(n,l)\Big) - \\ \Big(X(n,t) - X(n-l,t)\Big) F\Big(r(n,-l)\Big)\Big] - c_2,\end{aligned} \tag{50a}$$

$$\partial_t Y(n,t) = -\frac{\delta E}{\delta Y(n,t)}\,. \tag{50b}$$

Here the energy functional E has a form

$$E = \sum_{n=1}^{N} \mathcal{E}(n,t)\,, \tag{51}$$

where

$$\mathcal{E}(n,t) = \Big[\frac{1}{2}\, \nu\, Y^2(n,t) + \sum_{l=1,2} e^{-r(n,l)}\Big]\,. \tag{52}$$

is the energy density, and

$$r(n,l) = \sqrt{\Big(X(n,t) - X(n+l,t)\Big)^2 + \Big(Y(n,t) - (-1)^l Y(n+l,t)\Big)}$$

is a distance between particles n and $n+l$ expressed in terms of the smooth coordinates X and Y, and the function $F(x)$ is defined by Eq.(6) with $\alpha = 1$. Eqs. (50) should be augmented by the constraint

$$X(N+1,t) - X(1,t) = aN \tag{53}$$

which expresses the conservation of the total longitudinal distance between particles.

A perturbation of the two-lane flow is given by

$$\begin{pmatrix} X(n,t) \\ Y(n,t) \end{pmatrix} = \begin{pmatrix} a\,n + U_1(n,t) \\ \frac{b}{2} + U_2(n,t)) \end{pmatrix} \tag{54}$$

with the conditions

$$U_\alpha(n+N,t) = U_\alpha(n,t), \quad \alpha = 1,2\,, \quad \forall n\,.$$

Writing

$$U(n,t) = \begin{pmatrix} U_1(n,t) \\ U_2(n,t) \end{pmatrix} \in \mathbb{R}^2 \tag{55}$$

and taking the Fourier transform

$$U(n,t) = \sum_k e^{iks}\,\hat{U}(k,t)\,, \tag{56}$$

with

$$\hat{U}(k,t) = \begin{pmatrix} \hat{U}_1(k,t) \\ \hat{U}_2(k,t) \end{pmatrix} \in \mathbb{C}^2\,,\ \hat{U}(-k,t) = \hat{U}^*(k,t)\,, \tag{57}$$

the system (50) reduces to the system

$$\partial_t \hat{U}(k,t) = M(k)\hat{U}(k,t) + \mathcal{N}(k,t). \tag{58}$$

Here, the matrices $M(k)$ are given by

$$M(k) = \begin{pmatrix} M_{11}(k) & M_{12}(k) \\ M_{21}(k) & M_{22}(k) \end{pmatrix} \tag{59}$$

with

$$\begin{aligned}
M_{11}(k) &= 4\sin^2\left(\frac{k}{2}\right)\left(\frac{a^2F'(\xi)}{\xi} + 4e^{-2a}\sin^2\left(\frac{k}{2}\right) - 4e^{-2a} + F(\xi)\right) \\
&\quad + 2i\epsilon\sin(k)\left(-\frac{a^2F'(\xi)}{\xi} + 2e^{-2a}\cos(k) - F(\xi)\right), \\
M_{12}(k) &= -\frac{4ab\epsilon\cos^2\left(\frac{k}{2}\right)F'(\xi)}{\xi} - \frac{2iab\sin(k)F'(\xi)}{\xi}, \\
M_{21}(k) &= \frac{2iab\sin(k)F'(\xi)}{\xi}, \\
M_{22}(k) &= \frac{2e^{-2a}\sin^2(k)}{a} + 4\cos^2\left(\frac{k}{2}\right)\left(\frac{b^2F'(\xi)}{\xi} + F(\xi)\right) - \nu\,,
\end{aligned} \tag{60}$$

where the abbreviation $\xi = \sqrt{a^2+b^2}$ is used, and the nonlinearity

$$\mathcal{N}(k) = \begin{pmatrix} \mathcal{N}_1(k) \\ \mathcal{N}_2(k) \end{pmatrix}\,, \tag{61}$$

is at least quadratic so that $\mathcal{N}_\alpha(k) = \mathcal{O}(|U|^2)$.

By considering the linear part of the problem, we are looking for solutions in the form

$$U(k) = \hat{U}(k)\,e^{z(k)t}, \tag{62}$$

where $\hat{U}(k)$ are constant amplitudes and the complex rate constants $z(k)$ are the eigenvalues for the matrices $M(k)$:

$$\sum_{\beta=1,2} M_{\alpha\beta}(k)\, B_{\beta\mu}(k) = z_\mu(k)\, B_{\alpha\mu}(k), \quad \mu = 1,2 \tag{63}$$

with $B_{\alpha\mu}(k)$ being the corresponding eigenvectors. They are given by

$$z_\mu(k) = \frac{M_{11}(k) + M_{22}(k)}{2} + (-1)^\mu \sqrt{\frac{1}{4}\Big(M_{11}(k) - M_{22}(k)\Big)^2 + M_{12}(k)\, M_{21}(k)}, \tag{64a}$$

$$\Big(B_{1\mu}(k), B_{2\mu}(k)\Big) = \Big(\frac{M_{12}(k)}{z_\mu(k) - M_{11}(k)}, 1\Big), \quad \mu = 1,2\,. \tag{64b}$$

The two-lane free flow is unstable if there exists an eigenvalue $z_\mu(k)$ for which $\Re\Big(z_\mu(k)\Big) > 0$.

By inserting Eq. (6) into Eq. (64a), one can conclude that the curve

$$a = f_r(\nu)\,, \qquad f_r(\nu) = W\left(\frac{4}{\nu}\right)\,, \tag{65}$$

determines the stability boundary with respect to the linear mode $k = 0$ or, in other words, the curve (65) separates the two-lane regime and the one-lane regime. The curve

$$a = f_l(\nu)\,, \qquad f_l(\nu) = W\left(\frac{4}{\nu}\right)\left[1 + W\left(\frac{4}{\nu}\right)\right]^{-\frac{1}{2}} \tag{66}$$

gives the stability boundary with respect to staggered linear modes with $k = \pm\pi$ and corresponds to the transition to a so-called unsorted motion (see Fig. 1(d)) where particles can overtake each other and strictly speaking, is beyond the scope of the model.

5.2. **Peristaltic domain.** In the area of existence of the two-lane regime which is bounded by the curves (65) and (66)

$$f_l(\nu) < a < f_r(\nu) \tag{67}$$

there is a domain where $\Re\Big(z_2(k)\Big) > 0$ in a finite interval of the wave number $0 < k \le k_c$ (see Fig. 3(a)) while $\Re\Big(z_1(k)\Big) < 0$ for all $k \in (0,\pi)$.

This means that the two-lane flow is unstable in this domain with respect to the linear modes $\mu = 2$ with $0 < k \le k_c$. Note that in the framework of a similar model but with another type of particle interactions the spatially inhomogenous stationary states in the case of the symmetric interaction $\epsilon = 0$ are discussed in [6]. The shape of the instability domain depends on the asymmetry of the interaction and the number of particles N (see Figs. 4 and 5). It is worth mentioning that the boundaries of the peristaltic domain (blue area in Figs. 4 and 5) correspond to the two-lane state instability with respect to the first harmonics of the mode $\mu = 2$, *i.e.* they are described by the function $\Re\Big(z_2(\frac{2\pi}{N})\Big) = 0$. This is illustrated in Fig. 3(b) where the growth rates of the first three harmonics of the linear mode with $\mu = 2$ are shown as a function of the mean interparticle distance a. The first harmonics with $k = 2\pi/N$ is unstable in the interval $a \in (a_l, a_r)$ where the parameters a_l and a_r are functions of the asymmetry parameter ϵ, the strength of the interaction with walls ν, and the number of particles N. As it was discussed

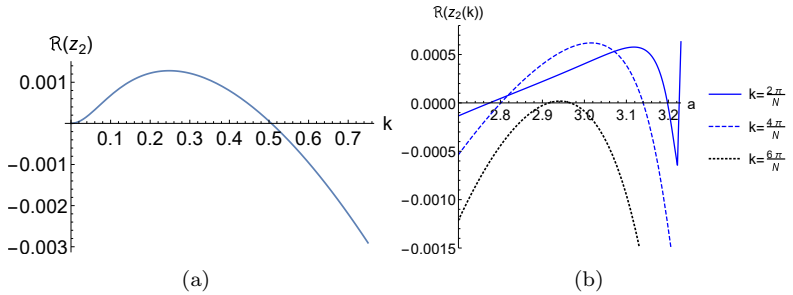

FIGURE 3. Panel (a): the growth rate $\Re(z_2)$ of the linear mode $\mu = 2$ *vs* the wave number k. Panel (b): the growth rate of the first three harmonics of the linear mode $\mu = 2$ *vs* the mean interparticle distance a. In both figures $\epsilon = 0.5, \nu = 0.05, N = 32$.

above the phase transition 2-lane→1-lane is due to instability with respect to the mode $k = 0$. Therefore, it is understandable why the distance $f_r - a_r$ between the right boundary of the peristaltic domain and the boundary which separates 1-lane and 2-lane free flow regimes decreases when the number of particles N increases (compare Figs. 4 and 5).

To characterize the behavior of the system in the peristaltic domain it is convenient to introduce a quantity which plays a role of an order parameter. This quantity is defined as follows

$$R = \sqrt{\frac{1}{N}\sum_{n=1}^{N} sY^2(n,t) - \Big(\frac{1}{N}\sum_{n=1}^{N} sY(n,t)\Big)^2} \equiv \sqrt{\sum_{j=1}^{N/2} |\widehat{sY}(\frac{2\pi}{N}\, j, t)|^2}\,, \qquad (68)$$

where

$$\widehat{sY}(k,t) = \frac{1}{N}\sum_{n} sY(n,t)\, e^{-ikn}\,, \qquad k = \frac{2\pi}{N}\, j \qquad (69)$$

is the Fourier transform of the transversal distance $sY(n,t) = Y(n+1,t) + Y(n,t)$. The quantity R vanishes when the flow is spatially homogeneous: $sY(n,t) = b$, and it is finite when the flow is spatially inhomogeneous. Bifurcation diagrams in the $\Big(1/\rho, R\Big)$ plane for symmetric (panel(a)) and asymmetric (panel(b)) interparticle interaction are shown in Fig. 6. In particular, we note in Fig. 6 that the bifurcation, which occurs at the left boundary of the peristaltic domain, is subcritical with a wide hysteretic interval, while the bifurcation at the right boundary is either supercritical for the case of symmetric interparticle interaction $\epsilon = 0$ (see Fig. 6(a)) or weakly subcritical with narrow hysteretic interval (see Fig. 6(b)) for the asymmetric interparticle interaction.

6. **Spatio-temporal peristaltic evolution in the collective coordinate approach.**

6.1. **Localized states in systems with symmetric interparticle interaction: $\epsilon = 0$.**

First we consider the case of the symmetric social interaction. Numerical solution of the equations (9) show that when the density of pedestrians ρ and the strength of pedestrian-wall interaction ν are in the blue area in Figs. 4(a) and 5(a)

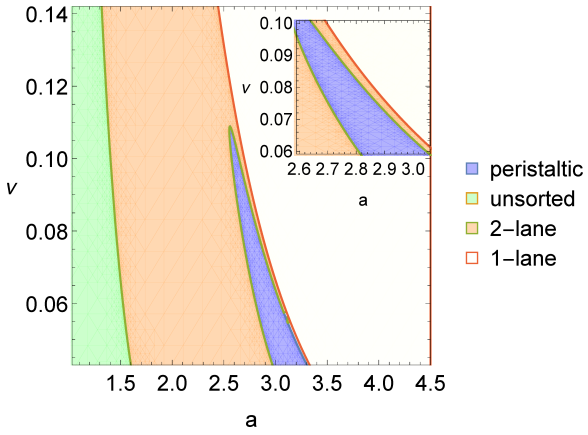

(a) $\epsilon = 0$

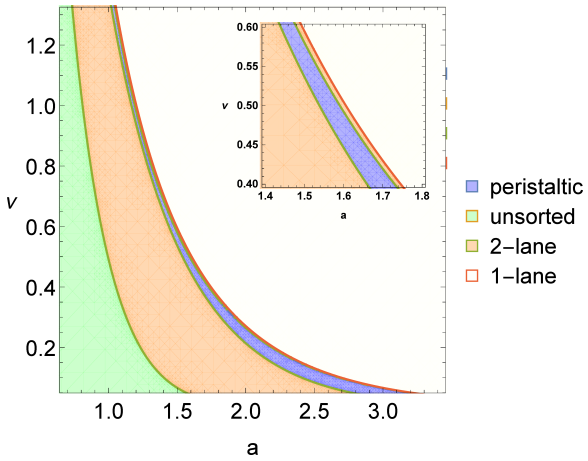

(b) $\epsilon = 0.5$

FIGURE 4. Bifurcation diagrams obtained from the linear stability analysis for $N = 32$ and the asymmetry parameter $\epsilon = 0$ (panel (a)) and $\epsilon = 0.5$ (panel (b)). Insets show details of the diagram in the vicinity of the two-lane regime instability. In the white (orange) area the one- (two-) lane flow is stable. In the blue area we observe the peristaltic regime and the distance between lanes is spatially and time modulated, in the green area the two-lane flow is linearly unstable, and the instability leads to unsorted motion as shown in Fig. 1(d).

the stationary state of the system is a spatially inhomogeneous mixed state: one part of agents moves in one-lane flow, while the rest of agents create a two-lane flow (see Figs. 7 and 8). The aim of this section is to show that in the area of consideration the mixed state is energetically more preferable than the spatially uniform one- and two-lane states.

In the case of symmetric social interaction the dynamics of the system is variational:

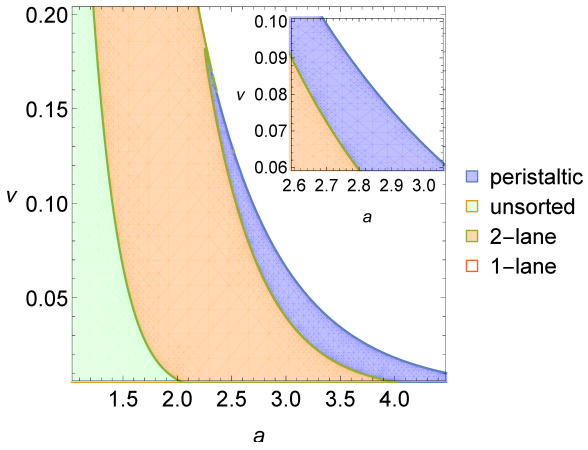

(a) $\epsilon = 0$

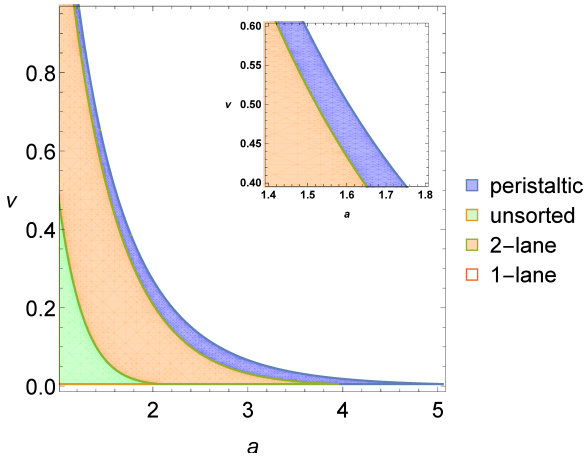

(b) $\epsilon = 0$.

FIGURE 5. The same as in Fig. 4 for $N = 128$.

$$\partial_t X(n,t) = -\frac{\delta E}{\delta X(n,t)},$$
$$\partial_t Y(n,t) = -\frac{\delta E}{\delta Y(n,t)}. \tag{70}$$

where the energy functional E is given by Eqs. (51) and (52).

It is impossible to find analytically stationary distribution of particles in the whole interval of existence of the peristaltic regime. To obtain a general picture of the mixed state behavior we will use a variational approach. Afterwards we find localized solutions corresponding to the energy functional (51), (52) in a weak nonlinearity limit.

Being motivated by the results of our numerical simulations presented in Figs. 7 and 8, we look for stationary solutions of Eqs. (70), *i.e.* extrema of the functional

(51), by using the following ansatz

$$\begin{aligned} X(n) &= n\,a_1 - \frac{a_1 - a_2}{2\,\kappa}\,\ln\Big(\frac{\cosh\kappa\,(n-n_0)}{\cosh\kappa\,(n-n_1)}\Big), \\ Y(n) &= y\,\frac{1}{2}\Big[\tanh\Big(\kappa\,(n-n_0)\Big) - \tanh\Big(\kappa\,(n-n_1)\Big)\Big], \end{aligned} \tag{71}$$

which describes the mixed phase where pedestrian in the interval $n \in (n_0, n_1)$ create a two-lane profile (with the distance between lanes y and the headway a_2) while the rest of pedestrian create the one-lane profile with the headway a_1. Here a_1, a_2, y, κ are variational parameters. Note that the mean density of pedestrians $\rho = 1/a$ is constant and therefore the parameters a_1 and a_2 are coupled by the relation (53) which in the limit

$$N \gg 1,\ \zeta \equiv \frac{n_1 - n_0}{N} = \mathcal{O}(1) \tag{72}$$

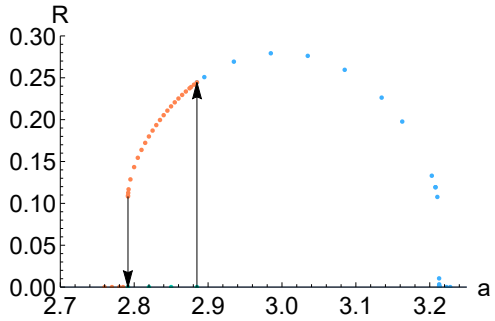

(a) $R(a)$ for fixed $\nu = 0.05$ and $\epsilon = 0$

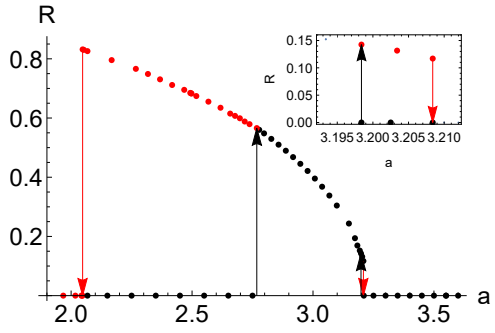

(b) $R(a)$ for fixed $\nu = 0.05$ and $\epsilon = 0.5$

FIGURE 6. The order parameter R of the peristaltic phase vs. mean headway, a, for fixed $\nu = 0.05$. Panel (a): R vs. a, in the case of totally symmetric social interaction $\epsilon = 0$: panel (b) R vs. a, in the case of partially asymmetric social interaction: $\epsilon = 0.5$. Panel (a): in the region between arrows a hysteretic behavior takes place: red-dot-curve presents downsweep stable branch, black-dot-curve presents upsweep stable branch. Panel (b): as in panel (a); the inset shows the hysteretic behavior near the right boundary of the peristaltic phase $a = 3.198$.

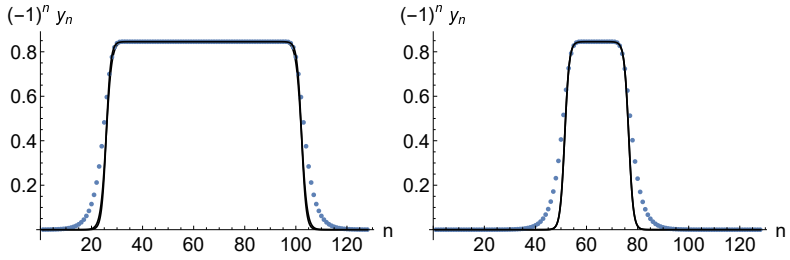

(a) $a = 2.93$ (b) $a = 3.13$

FIGURE 7. Staggered transversal coordinates $(-1)^n y_n$ in the mixed phase state for two different values of the pedestrian headway: $a = 2.93$ (panel (a)) and $a = 3.13$ (panel (b)). The social interaction is symmetric: $\epsilon = 0$. Other parameters are chosen inside the domain of mixed phases state: $\nu = 0.05$, $N = 128$. The solid lines represent the results obtained in the frame of the analytical approach, the dots represent the results of numerical solutions of Eqs. (9).

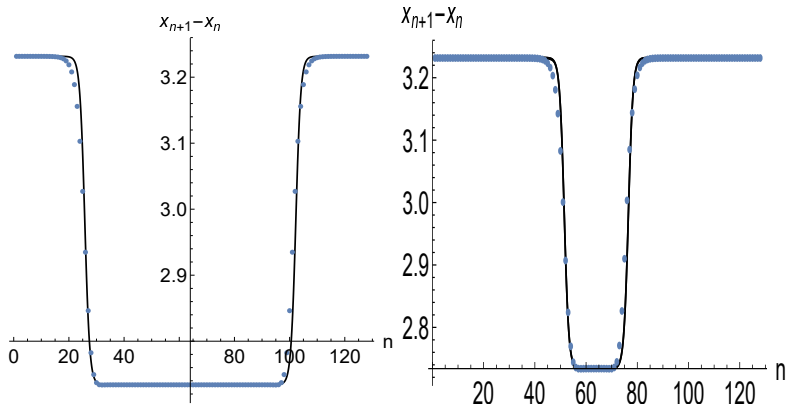

(a) $a = 2.93$ (b) $a = 3.13$

FIGURE 8. Longitudinal distances between nearest neighbors $x_{n+1} - x_n$ in the mixed phase state. All parameters are the same as in Fig. 7.

reduces to

$$\zeta\, a_2 + (1-\zeta)\, a_1 = a \quad \text{or} \quad a_1 = (a - \zeta\, a_2)/(1-\zeta) \tag{73}$$

The parameter ζ gives the portion of pedestrians in the two-lane phase. In the limit $N \gg 1$ it is coupled with the order parameter R introduced by Eq. (68) by the relation $R = \sqrt{\zeta(1-\zeta)}$.

By inserting the ansatz (71) into Eq. (51), one can obtain that the energy per particle of the mixed state consists of two parts

$$\tfrac{E}{N} \quad = \mathcal{E}(\zeta, a_2, y) + \mathcal{E}_b(\zeta, a_2, y, \kappa)\ . \tag{74}$$

Here

$$\mathcal{E}(\zeta, a_2, y) = (1-\zeta)\left(e^{-a_1} + e^{-2a_1}\right) + \zeta\left(e^{-\sqrt{a_2^2+4y^2}} + e^{-2\,a_2}\right) + \tfrac{1}{2}\,\zeta\,\nu\,y^2 \quad (75)$$

is the bulk part of the energy, where the mean distance between particles in the one-lane phase a_1 is given by Eq. (73), and

$$\mathcal{E}_b(\zeta, a_2, y, \kappa) = \frac{E}{N} - \mathcal{E}(\zeta, a_2, y) \quad (76)$$

is the energy cost for creating boundaries between one-lane and two-lane phases.

We are interested in the case when the number of pedestrians is large: $N \gg 1$. In this limit by looking for minimum of the functional given by Eqs. (51), (52) with respect to the variational parameters ζ, a_2 and y, one can consider the energy term $\mathcal{E}_b$ as a small perturbation.

The extrema of the function (75) are determined by the expressions

$$y = \tfrac{1}{2}\sqrt{W^2(4/\nu) - a_2^2}\,, \qquad \zeta = \frac{a_3 - a}{a_3 - a_2}\,, \quad (77)$$

where the expression

$$a_3 = -\log\left(\frac{1}{4}\left(\sqrt{2a_2\nu + 16e^{-2a_2} + 1} - 1\right)\right) \quad (78)$$

gives a longitudinal interparticle distance at which the mixed phase transforms to the one-lane phase ($\zeta = 0$). The equilibrium interparticle distance in the two-lane phase a_2 depends solely on the strength of interaction with walls ν and is given by an implicit function

$$\begin{gathered}\nu\,a_2\,(a_2 - 1) - \sqrt{2a_2\nu + 16e^{-2a_2} + 1} + \\ \left(2a_2\nu + 16e^{-2a_2}\right)\ln\left(\tfrac{1}{4}\left(\sqrt{2a_2\nu + 16e^{-2a_2} + 1} - 1\right)\right) + \\ 16e^{-2a_2}a_2 + \nu W^2\left(\tfrac{4}{\nu}\right) + 2\nu\,W\left(\tfrac{4}{\nu}\right) + 1 = 0\,. \end{gathered} \quad (79)$$

As it follows from Eqs. (77) and (17) for $a = a_2$, $\zeta = 1$ and $y = b/2$. For this value of the headway the energy of the system given by Eq. (75) coincides with the energy of the spatially homogeneous two-lane state $\mathcal{E}(1, a, b)$. Thus, at $a = a_2$ the system undergoes a transition: peristaltic(mixed)-phase$\rightarrow$ two-lane phase. Note that in the framework of the collective coordinate approach the interval of existence of the peristaltic phase (a_2, a_3) is wider than the interval (a_l, a_r) which follows from the linear stability analysis discussed in Sec. 5.

The mixed phase is energetically more favorable in the parameter domain where the energy difference

$$\Delta\mathcal{E} = \mathcal{E}(\zeta, a_2, y) - \mathcal{E}(1, a, b) \quad (80)$$

is negative. Fig. 9 shows that the mixed phase is energetically preferable in the most part of the interval (a_2, a_3) and only in the vicinity of $a = a_3$ the energy difference is positive. In this area the ansatz (71) does not work (see below).

The stationary value of the inverse width κ is determined by the equation

$$\partial_\kappa \mathcal{E}_b = 0. \quad (81)$$

The solution of this equation is presented in Fig. 10. The parameters ζ, y, a_2, which were used in this equation, were taken from Eqs. (77) and (79). Fig. 10 shows that when $a > a_{cr}$ where a_{cr} gives the point of the intersection of the curves $\partial_\kappa \mathcal{E}_b = 0$ and $\partial_\kappa^2 \mathcal{E}_b = 0$, the energy of the system has a minimum with respect to all variational parameters. At $a = a_{cr}$ the minimum of the energy with respect to the inverse width ceases to exist and instead of the minimum the energy has a saddle point.

The critical value $a_{cr} = 2.79$ is very close to the critical value of the existence of the persistaltic phase obtained from the bifurction analysis (see Fig. 6). This explains the subcritical behavior of the order parameter in the framework of the variational approach.

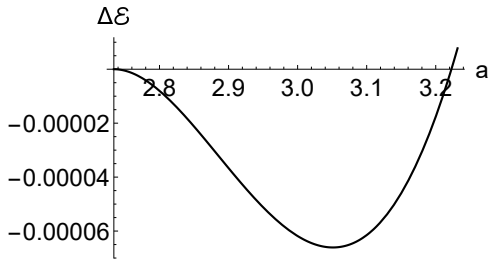

FIGURE 9. Energy difference between the mixed state and the spatially homogeneous two-lane state as a function of the mean headway a in the interval $a \in (a_2, a_3)$. The social interaction is symmetric $\epsilon = 0$, the pedestrian-wall interaction is fixed: $\nu = 0.05$.

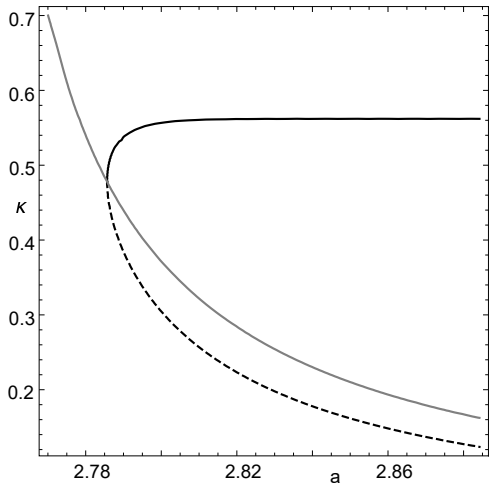

FIGURE 10. The stationary value of the inverse width κ vs the mean distance a obtained from Eq. (81). The solid (dashed) curve presents a stable (unstable) solution. The curves are plotted in the mean distance interval $a \in (a_2, a_l)$, where the mixed phase is unstable in the linear anaylsis aproach and it is stable in the frame of the variational approach. The solid line gives the contour, where $\partial^2_\kappa \mathcal{E}_b = 0$. The social interaction is symmetric $\epsilon = 0$, the pedestrian-wall interaction is fixed: $\nu = 0.05$.

Equation (77) shows that the equilibrium portion of the two-lane phase for a given value of the intensity of the interaction with walls increases when the pedestrian density ρ increases. This is also seen from Figs. 7 and 8 where pedestrian flow profiles are shown for the same values of the pedestrian density. As one can also see from these figures the results of full scale numerical simulations (dots) and analytical results (solid lines) are in a rather good agreement.

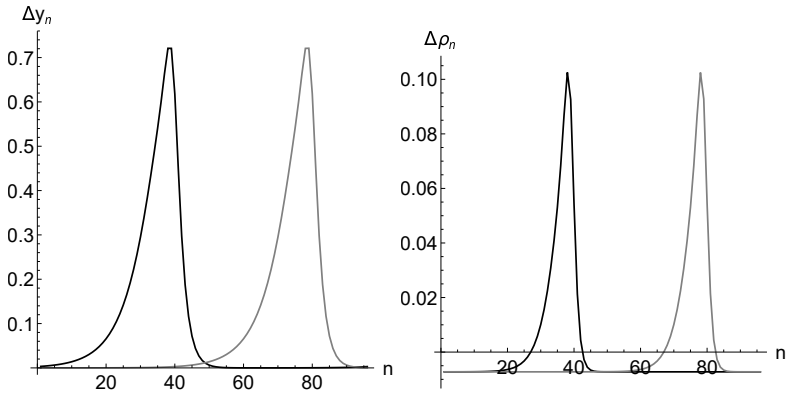

(a) Distance between lanes (b) Excess of density

FIGURE 11. Spatio-temporal evolution of the local distance between lanes $\Delta y_n = |y_{n+1} - y_n|$ (panel (a)) and the excess density $\Delta\rho_n = \frac{1}{x_{n+1}-x_n} - \frac{1}{a}$ (panel (b)) for totally asymmetric social interaction ($\epsilon = 1$). Other parameters are chosen inside the domain of peristaltic motion: $a = 1.4$, $\nu = 0.65$. The two profiles are separated by the time difference $\Delta t = 250$.

6.2. **Asymmetric social interaction.** One of interesting features of pedestrian dynamics with asymmetric social interaction is the appearance of bubble-like distributions which propagate along the corridor with a constant velocity by preserving their shape (see Fig. 11). It is of interest therefore to clarify what does determine the velocity of the bubble. To this end we first to transfer Eqs. (50) to a new moving frame of reference

$$X(n,t) = (c_2 + \tilde{c})t + \tilde{X}(n,t) \tag{82}$$

where the velocity $\tilde{c}$ will be specified below. We extend Eq. (9) by allowing n to be a continuous variable. We consider an infinitely long corridor: $-\infty < n < \infty$ and assume that the functions $\tilde{X}(n,t)$ and $Y(n,t)$ satisfy the following boundary conditions

$$\tilde{X}(n,t) \to na_1, \quad Y(s,t) \to 0, \quad \text{for} \quad n \to \pm\infty \tag{83}$$

where a_1 is an asymptotic distance between nearest pedestrians. The functions $\tilde{X}(s,t)$ and $Y(s,t)$ satisfy the equations

$$\begin{aligned}\partial_t \tilde{X}(n,t) + \frac{\delta E}{\delta \tilde{X}} = \epsilon \sum_{i=1}^{2} \Big[\Big(\tilde{X}(n,t) - \tilde{X}(n+i,t)\Big) F\Big(r(n,i)\Big) - \\ \Big(\tilde{X}(n,t) - \tilde{X}(n-i,t)\Big) F\Big(r(n,-i)\Big)\Big] - \tilde{c},\end{aligned} \tag{84a}$$

$$\partial_t Y(s,t) = -\frac{\delta E}{\delta Y}\,, \tag{84b}$$

where the function $F(x)$ is defined by Eq. (6) with $\alpha = 1$, and E is a continuum analog of the energy of the system in the case of the symmetric social interaction (51), (52).

To make Eq. (84a) consistent with the boundary conditions (83) the velocity $\tilde{c}$ has to be chosen in the form

$$\tilde{c} = -2\,\epsilon\left(e^{-a_1} + e^{-2a_1}\right). \tag{85}$$

By multiplying Eq. (84a) by $\partial_n \tilde{X}$ and Eq. (84b) by $\partial_n Y$ and summing and integrating them up, one can obtain that the quantity

$$P = \int\limits_{-\infty}^{\infty} \Big(\partial_t \tilde{X}\,\partial_n \tilde{X} + \partial_t Y\,\partial_n Y\Big) dn\,, \tag{86}$$

which has a meaning of momentum, follows a balance equation

$$\begin{aligned} P = \epsilon \int\limits_{-\infty}^{\infty} \Big\{\partial_n \tilde{X} \sum_{i=1}^{2} \Big[\Big(\tilde{X}(n,t) - \tilde{X}(n+i,t)\Big)\, F\Big(r(n,i)\Big) - \\ \Big(\tilde{X}(n,t) - \tilde{X}(n-i,t)\Big)\, F\Big(r(n,-i)\Big) + 2\Big(e^{-a_1} + e^{-2a_1}\Big)\Big]\Big\}\, dn\,. \end{aligned} \tag{87}$$

We consider a weakly asymmetric case: $\epsilon \ll 1$. In this case, being interested in a speed with which the peristaltic pulse propagates along the corridor, one can neglect the change of the profile shape caused by the asymmetry of the social interaction and as a traveling wave ansatz use Eq. (71) with

$$n_0 = \xi(t) - \frac{1}{2}\,\zeta\, N, \quad n_1 = \xi(t) + \frac{1}{2}\,\zeta\, N, \tag{88}$$

where $\xi(t)$ is a center of mass coordinate and $\zeta\, N = n_1 - n_0$ is the length of the two-lane region (see Eq.(72)). By substituting Eqs. (71), (88) into Eqs. (86), we get

$$P = -\frac{d\xi}{dt} \int\limits_{-\infty}^{\infty} \Big[\Big(-a_1 + \partial_n \tilde{X}\Big)\,\partial_n \tilde{X} + \Big(\partial_n Y\Big)^2\Big] dn\,. \tag{89}$$

When the functions $X(n,t)$ and $Y(n,t)$ are smooth, the finite differences in Eq. (87) can be approximated by

$$X(n+i,t) - X(n,t) \approx i\,\partial_n X, \quad Y(n+i,t) - Y(n,t) \approx i\,\partial_n Y \tag{90}$$

and by substituting Eqs. (89) and (90) into the balance equation (87) one can obtain that the velocity of the peristaltic pulse in the limit (72) is given by the following approximate expression

$$\frac{d\xi}{dt} = 2\epsilon\,\frac{1-\zeta}{a_2 - a}\left(\frac{1}{4}\,\nu\, a_2 + e^{-2a_2} - e^{-a_1} - e^{-2a_1}\right) + \mathcal{O}\Big(\frac{1}{\kappa\,\zeta\, N}\Big) \tag{91}$$

where the parameters a_1, a_2 and ζ are given by Eqs. (73), (77) and (79). The function $\frac{d\xi}{dt}$ from (91) and its comparison with full scale numerical simulations is presented in Fig. 12. It can be seen that there is good agreement between numerics and the analysis in the main part of the existence of the peristaltic phase except at close vicinity to the right boundary. In the vicinity of the right boundary the ansatz (71) does not work and a new approach has to be developed.

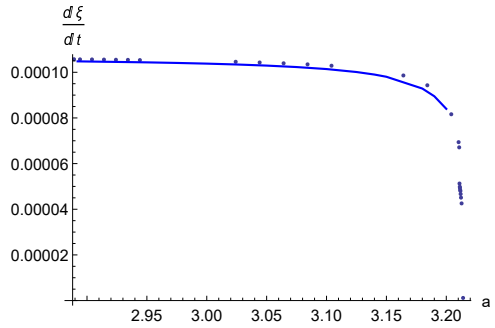

FIGURE 12. Velocity of the peristaltic pulse as a function of the inverse density. Comparison of the analytical results obtained from Eq. (90) (solid curve) and full scale numerical results (dots). The social interaction is weakly asymmetric $\epsilon = 0.01$, the pedestrian-wall interaction is fixed: $\nu = 0.05$, the number of pedestrian $N = 128$.

7. **Spatio-temporal peristaltic evolution in the continuum approach.** It was mentioned above that the ansatz given by Eq. (71) does not work in the close vicinity of the right boundary of the peristaltic domain. In this section we present a derivation of an effective equation, which describes the spatio-temporal evolution of the system in the near-critical region: *i.e.* in the area where the parameters (ρ, ν) belong to the right boundary region, which separates the peristaltic regime and the free two-lane regime. As it follows from the numerical simulations the bifurcation at this boundary is weakly sub-critical (see Fig. 6), the amplitudes of the peristaltic pulses are small and their spatial variation is smooth. By using the scaling with the scaling parameter $\eta \ll 1$

$$Z(n,t) \equiv X(n,t) - a\,n \sim \eta, \qquad Y(n,t) \sim \eta, \qquad \partial_n \sim \eta,$$
$$\partial_t \sim \eta^2, \qquad \tfrac{4e^{-a}}{a} - \nu \sim \eta^2\,, \tag{92}$$

and assuming that the asymmetry of the interparticle interaction is weak: $\epsilon \sim \eta$, with the accuracy $\mathcal{O}(\eta^2)$ one can obtain from Eqs. (50) that the dynamics of the system is governed by the set of equations

$$\partial_t Z(n,t) = \partial_n \left(g_1 \partial_n Z(n,t) + g_2 Y^2(n,t)\right) + 2\,\epsilon \left(g_3 \partial_n Z(n,t) + g_2 Y^2(n,t)\right), \tag{93}$$

$$\partial_t Y(n,t) = h_1\,\partial_n^2 Y(n,t) + h_0 Y(n,t) - 2 g_2\, Y(n,t) \partial_n Z(n,t) - h_2\, Y^3(n,t), \tag{94}$$

where the notations

$$g_1 = 4e^{-2a} + e^{-a}, \quad g_2 = \frac{2(a+1)e^{-a}}{a^2}, \quad g_3 = 2e^{-2a} + e^{-a}, \tag{95}$$

$$h_0 = \frac{4e^{-a}}{a} - \nu, \quad h_1 = \frac{e^{-a} - 2e^{-2a}}{a}, \quad h_2 = 4\,\frac{g_2}{a} \tag{96}$$

are introduced. In terms of the variable $Z(n,t)$ the constraint given by Eq. (53) reduces to

$$\int_0^N \partial_n Z(n,t)\, dn = 0 \tag{97}$$

7.1. **Symmetric interparticle interaction.** Let us consider first the stationary solutions of Eqs. (93) and (94) in the case of the symmetric interparticle interaction: $\epsilon = 0$. The stationary solutions satisfy the equations

$$\partial_n \left(g_1 \partial_n Z + g_2 Y^2 \right) = 0 \,, \tag{98a}$$

$$h_1 \, \partial_n^2 Y + h_0 Y - 2 g_2 \, Y \partial_n Z - h_2 \, Y^3 = 0. \tag{98b}$$

By taking into account the constraint (97), from Eq. (98a) we get

$$\partial_n Z(n) = \frac{g_2}{g_1} \Big(C - Y^2 \Big) \tag{99}$$

where

$$C = \langle Y^2 \rangle \equiv \frac{1}{N} \int_0^N Y^2(n) \, dn \tag{100}$$

is a nonlocal functional of the patterm $Y(n)$. Note that the spatio-inhomogeneous stationary solutions in a closely related model of repulsive particles was quite recently considered in Ref. [6]. In Ref. [6] equations similar to Eqs. (98) were derived and analyzed. However, the constraint (97) was ignored (in Ref. [6] the constant C was chosen equal to zero) and therefore the results obtained in Ref. [6] differ from ours.

Substituting Eq. (99) into Eq. (98b), we obtain the nonlocal equation

$$h_1 \partial_n^2 Y + \left(h_0 - 2 \, \frac{g_2^2}{g_1} \, \langle Y^2 \rangle \right) Y + \left(2 \, \frac{g_2^2}{g_1} - h_2 \right) Y^3 = 0. \tag{101}$$

We are interested in solutions of Eq. (101), which satisfy the periodicity condition

$$Y(s + N) = Y(s). \tag{102}$$

The function

$$Y(n) = B \, \mathrm{dn}(\varkappa n, m), \tag{103}$$

where $\mathrm{dn}(z, m)$ is the Jacobi dn-function with modulus m [1],

$$B = \sqrt{\frac{2}{2 - m} \, \frac{2 \, C \, g_2^2 - g_1 \, h_0}{2 \, g_2^2 - g_1 \, h_1}}, \quad \varkappa = \sqrt{\frac{2 \, C \, g_2^2 - g_1 \, h_0}{(2 - m) \, g_1 \, h_2}}, \tag{104}$$

satisfies Eq. (101). From the periodicity condition (102) and the constraint (100) we have, respectively

$$\varkappa = 2 \frac{K(m)}{N}, \tag{105}$$

and

$$C = B^2 \frac{E(m)}{K(m)}, \tag{106}$$

where $K(m)$ and $E(m)$ are the complete elliptic integrals of the first and second kind, respectively [1].

By inserting Eqs. (95) and (104) into Eqs. (105), (106) we obtain that the modulus of the elliptic *dn*-function is determined by the equation

$$2 \sqrt{\frac{e^{-a} \, (e^a - 2) \, K(m) \, ((e^a - 4a) \, (m - 2) K(m) + 2(a + 1) e^a E(m))}{(e^a - 4a) \, (4 - a e^a \nu)}} = N \tag{107}$$

while the constraint constant C is given by

$$C = \frac{a^3\,(e^a+4)\,(ae^a\nu-4)\,E(m)}{4(a+1)\,((e^a-4a)\,(2-m)K(m)-2(a+1)e^aE(m))}\,. \tag{108}$$

For given ν, a and N there are two solutions of Eq. (107) (see Fig. 13(a)), which differ by their shape and energy; see Fig. 14 and Fig. 13(b). The solid line on Fig. 13(a) represents a stationary pattern, which is energetically more favorable than the solution, which corresponds to the dashed line. For $a < a_r$ with a_r being the right boundary of the interval $a \in (a_l, a_r)$, where the peristaltic phase exists, the spatially inhomogeneous pattern given by Eqs. (103), (107) and (108) is energetically more favorable than the uniform two-lane state. In the close vicinity of the right boundary a_r we observe a bistability of the spatially localized patterns in Fig. 13(b). The profiles obtained analytically in this section are in very good agreement with the results of full scale numerical simulations; see Fig. 15.

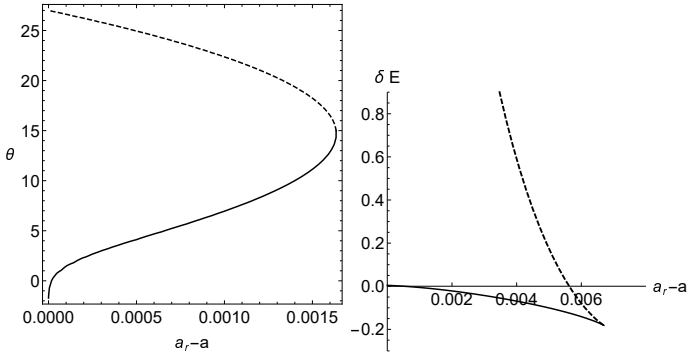

(a) $\theta \equiv \ln\frac{1-m}{m}$ *vs* a for fixed $\nu = 0.05$

(b) δE *vs* a for fixed $\nu = 0.05$

FIGURE 13. Panel (a): The modulus of elliptic function m vs. mean headway a, dashed line presents an energetically unstable branch. Panel (b): The dimensionless energy difference between the spatially homogeneous two-lane state and the peristaltic state $\delta E = (E_{per} - E_{two-lane})/|E_{two-lane}|$ vs. mean headway a. The critical headway a_r gives the right boundary of the peristaltic state stability interval. The two-lane state looses its stability and the peristaltic state is established for $a < a_r$. The solid and dashed lines correspond to two branches presented in panel (a).

Note that the constraint (97) and the corresponding effective nonlocal interaction play a crucial role in forming of the spatially localized pattern. In the presence of nonlocal interaction term in Eq. (101) the second term in Eq. (101) changes sign and it makes possible the appearance of stable spatially inhomogeneous patterns.

7.2. **Asymmetric interparticle interaction.** As mentioned in the previous section, in the presence of asymmetric interparticle interaction the "bubbles" move along the corridor by preserving their shape. In this subsection we evaluate a stationary velocity with which the bubble moves. To this end we similarly to Sec. 6.1

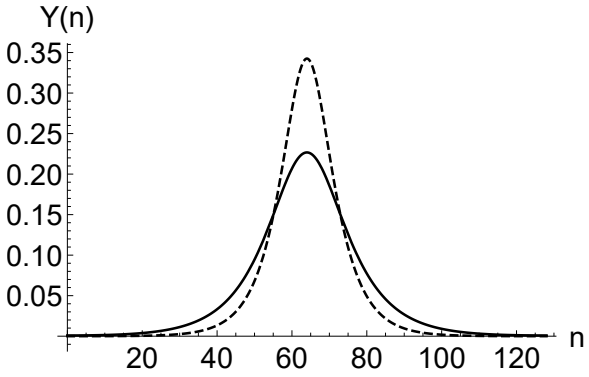

FIGURE 14. Two stationary localized solutions $Y(n)$ of Eq. (93) in the case of symmetric interparticle interaction for the mean headway $a = a_r - 0.0015$, the pedestrian-wall interaction $\nu = 0.05$. The number of pedestrian is $N = 128$. The solid line corresponds to the energetically more favorable state.

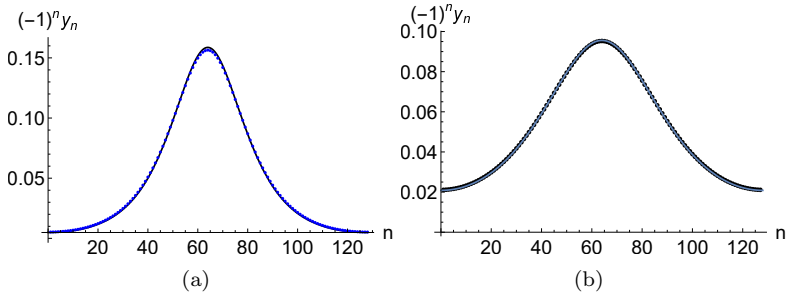

FIGURE 15. Staggered transversal coordinate $(-1)^n y_n$ profile obtained by numerical simulations (dots) and analytically from Eq. (103). The social interaction is symmetric $\epsilon = 0$, the number of particles is $N = 128$, the pedestrian-wall interaction is fixed: $\nu = 0.05$, the mean headway $a = a_r - 0.001$ (panel(a)), and $a = a_r - 0.0003$ (panel(b)).

will use the balance approach, which for the equation (93) has the form

$$\int_0^N \left(\partial_t Z \partial_n Z + \partial_t Y \partial_n Y\right) dn = 2\,\epsilon \int_0^N \partial_n Z \left(g_3 \partial_n Z(n,t) + g_2 Y^2(n,t)\right) dn\,. \quad (109)$$

We consider a weakly asymmetric case and will assume that the longitudinal and transversal coordinate profiles are the same as in the symmetric case. By substituting the traveling wave ansatz

$$Z(n,t) = Z(n - \xi(t)), \quad Y(n) = Y(n - \xi(t)). \quad (110)$$

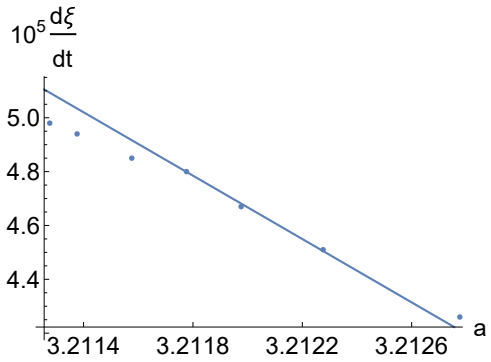

FIGURE 16. Pulse velocity in the vicinity of the bifurcation point a_r obtained from numerical solutions of Eq. (9) (dots) and from analysis (see Eq. (111)) in the case of weakly asymmetric interparticle interaction $\epsilon = 0.01$ for the mean headway $0 < a_r - a \ll 1$. The pedestrian-wall interaction is $\nu = 0.05$. The number of pedestrian is $N = 128$. See also Fig. 12.

with $Z(n)$ and $Y(n)$ given by Eqs. (99) and (103) in the balance equation (109) and carrying out integrations, we get

$$\frac{d\xi}{dt} = 2\,\epsilon\,(g_3 - g_1)\frac{\langle \mathrm{dn}^4\rangle - \langle \mathrm{dn}^2\rangle}{\langle \mathrm{dn}^4\rangle - \langle \mathrm{dn}^2\rangle + \frac{g_1}{h_1}\left(1 - \frac{g_1 h_2}{2g_2^2}\right)(m - 1 + (2-m)\langle \mathrm{dn}^2\rangle - \langle \mathrm{dn}^4\rangle)}, \quad (111)$$

where the abbreviations

$$\langle \mathrm{dn}^2\rangle = \frac{E(m)}{K(m)},$$
$$\langle \mathrm{dn}^4\rangle = \frac{(m-1)K(m) - 2(m-2)E(m)}{3K(m)} \quad (112)$$

are used. In the vicinity of the bifurcation point a_r one can expand the pulse velocity (111) in a Taylor series and as a result we get

$$\frac{d\xi}{dt} = \epsilon(\beta_0 + \beta_1(a_r - a)) \quad (113)$$

where the coefficients β_0 and β_1 are functions of the other parameters. Fig. 16 shows that the linear dependence of the velocity on the headway a is in qualitative agreement with results of full scale numerical simulations.

8. **Conclusions and outlook.** We have shown that a pedestrian model with asymmetric coupling incorporates various stable solutions, namely one- and two-lane flow, as well as a peristaltic motion. A linear stability analysis around the one- and two-lane flow revealed the location of stability boundaries and the transition to the peristaltic regime. The corresponding phase diagram has been obtained by the stability analysis and by parameter scans with direct numerical simulations. Both methods revealed the same behavior and are in agreement to a very high accuracy. To study the peristaltic motion we developed a collective coordinate approach, which gave a good agreement with numerics. Finally, we compared our findings of the peristaltic motion with an analogous continuum approach leading to the effective description of the motion by a nonlocal differential equation.

So far, we have only studied deterministic pedestrian dynamics by assuming that all pedestrians are identical and the velocity with which they intent to move (the first term in the right hand side of Eq. (1)) is the same for all pedestrians. It would be interesting to study a stochastic model, which takes into account the randomness of the intended velocity. In this paper we have considered asymmetric pedestrian dynamics in an ordered setup, i.e., all pedestrians have a fixed next-neighbor denoted by the labelling. It would be interesting to extend the definition of the model to the two-dimensional case where the next-neighbor might be chosen by a line-of-sight argument for each pedestrian. Similar approaches have already been made by [8, 17], where anisotropic force fields were studied. Furthermore, an extension to more complicated geometries, e.g., annuli [15, 26] and buildings, might be an interesting case for the asymmetric model.

Finally, the macroscopic dynamics of the pedestrian flow is worth studying with multiscale methods such as diffusion maps [22] or equation-free methods [19, 23, 24, 5]. A macroscopic analysis might find the observed transitions between regimes in a numerically simple way and could shed some light on the type of bifurcations by using a coarse bifurcation analysis.

Acknowledgments. YBG acknowledges a Guest Professorship funded by grants from Civilingeniør Frederik Christiansens Almennyttige Fond and from Otto Mønsteds Fond. He also acknowledges partial financial support from a special program of the National Academy of Sciences of Ukraine, and is thankful to the Department of Applied Mathematics and Computer Science, the Department of Physics, Technical University of Denmark and the School of Mathematical Sciences, Queen Mary University of London for hospitality. CM and JS are grateful for financial support of a research project by Civilingeniør Frederik Christiansens Almennyttige Fond.

REFERENCES

[1] M. Abramowitz and I. Stegun, *Handbook of Mathematical Functions*, Dover Publications, Inc., New York, 1966.
[2] N. Bellomo and C. Dogbe, On the modeling of traffic and crowds: A survey of models, speculations, and perspectives, *SIAM Review*, **53** (2011), 409–463.
[3] V. J. Blue and J. L. Adler, Cellular automata microsimulation for modeling bi-directional pedestrian walkways, *Transportation Research Part B*, **35** (2001), 293–312.
[4] C. Burstedde, K. Klauck, A. Schadschneider and J. Zittartz, Simulation of pedestrian dynamics using a two-dimensional cellular automaton, *Physica A*, **295** (2001), 507–525.
[5] O. Corradi, P. G. Hjorth and J. Starke, Equation-free detection and continuation of a Hopf bifurcation point in a particle model of pedestrian flow, *SIAM Journal on Applied Dynamical Systems*, **11** (2012), 1007–1032.
[6] T. Dessup, C. Coste and M. Saint Jean, Subcriticality of the zigzag transition: A nonlinear bifurcation analysis, *Physical Review E*, **91** (2015), 032917, 1–14.
[7] T. Dessup, T. Maimbourg, C. Coste and M. Saint Jean, Linear instability of a zigzag pattern, *Physical Review E*, **91** (2015), 022908, 1–12.
[8] F. Dietrich and G. Köster, Gradient navigation model for pedestrian dynamics, *Physical Review E*, **89** (2014), 062801, 1–8.
[9] J. E. Galván-Moya and F. M. Peeters, Ginzburg-Landau theory of the zigzag transition in quasi-one-dimensional classical Wigner crystals, *Physical Review B*, **84** (2011), 134106, 1–10.
[10] D. Helbing, Traffic and related self-driven many-particle systems, *Reviews of Modern Physics*, **73** (2001), 1067–1141.
[11] D. Helbing, P. Molnar, I. J. Farkas and K. Bolay, Self-organizing pedestrian movement, *Environment and Planning B-planning and Design*, **28** (2001), 361–383.

[12] D. Helbing and P. Molnar, Social force model for pedestrian dynamics, *Physical Review E*, **51** (1995), 4282–4286.
[13] D. Helbing, I. Farkas and T. Vicsek, Simulating dynamical features of escape panic, *Nature*, **407** (2000), 487–490.
[14] S. P. Hoogendoorn and W. Daamen, Pedestrian behavior at bottlenecks, *Transportation Science*, **39** (2005), 147–288.
[15] A. Jelić, C. Appert-Rolland, S. Lemercier and J. Pettré, Properties of pedestrians walking in line: Fundamental diagrams, *Physical Review E*, **85** (2012), 036111, 1–9.
[16] A. Johansson and D. Helbing, Crowd dynamics, in: *Econophysics and Sociophysics. Trends and Perspectives* (eds. B.K. Chakrabarti, A. Chakraborti and A. Chatterjee), Wiley-VCH, Weinheim, (2006), 449–472.
[17] A. Johansson, D. Helbing and P. K. Shukla, Specification of the social force pedestrian model by evolutionary adjustment to video tracking data, *Advances in Complex Systems*, **10** (2007), 271–288.
[18] B. S. Kerner, *The physics of Traffic: Empirical Freeway Pattern Features, Engineering Applications, and Theory*, 1^{st} edition, Springer-Verlag, Berlin Heidelberg, 2004.
[19] Y. G. Kevrekidis and G. Samaey, Equation-free multiscale computation: Algorithms and applications, *Annual Review of Physical Chemistry*, **60** (2009), 321–344.
[20] H.-K. Li, E. Urban, C. Noel, A. Chuang, Y. Xia, A. Ransford, B. Hemmerling, Y. Wang, T. Li, H. Häffner and X. Zhang, Realization of translational symmetry in trapped cold ion rings, *Physical Review Letters*, **118** (2017), 053001, 1–5.
[21] C. Marschler, J. Starke, M. P. Sørensen, Yu. Gaididei and P. L. Christiansen, Pattern formation in annular systems of repulsive particles, *Physics Letters A*, **380** (2016), 166–170.
[22] C. Marschler, J. Starke, P. Liu and Y. G. Kevrekidis, Coarse-grained particle model for pedestrian flow using diffusion maps, *Physical Review E*, **89** (2014), 013304, 1–11.
[23] C. Marschler, J. Sieber, P. G. Hjorth and J. Starke, Equation-free analysis of macroscopic behavior in traffic and pedestrian flow, in: *Traffic and Granular Flow '13* (eds. M. Chraibi, M. Boltes, A. Schadschneider and A. X. Armin Seyfried) Springer-Verlag, (2015), 423–439.
[24] C. Marschler, J. Sieber, R. Berkemer, A. Kawamoto and J. Starke, Implicit methods for equation-free analysis: Convergence results and analysis of emergent waves in microscopic traffic models, *SIAM Journal on Applied Dynamical Systems*, **13** (2014), 1202–1238, [http://arxiv.org/abs/1301.6044]
[25] J. E. Marsden and M. McCracken, *The Hopf Bifurcation and Its Applications*, Springer-Verlag, New York, 1976.
[26] M. Moussaïd, E.G. Guillot, M. Moreau, J. Fehrenbach, O. Chabiron, S. Lemercier, J. Pettré, C. Appert-Rolland, P. Degond and G. Theraulaz, Traffic Instabilities in Self-Organized Pedestrian Crowds, *PLoS Computational Biology*, **8** (2012), e1002442, 1–10.
[27] A. Schadschneider and A. Seyfried, Empirical results for pedestrian dynamics and their implications for modeling, *Networks and Heterogeneous media*, **6** (2011), 545–560.
[28] J. P. Schiffer, Phase transitions in anisotropically confined ionic crystals, *Physical Review Letters*, **70** (1993), 818–821.
[29] W. Tian, W. Song, J. Ma, Z. Fang, A. Seyfried and J. Liddle, Experimental study of pedestrian behaviors in a corridor based on digital image processing, *Fire Safety Journal*, **47** (2012), 8–15.
[30] T. Vicsek and A. Zafeiris, Collective motion, *Physics Reports*, **517** (2012), 71–140.
[31] D. E. Wolf, M. Schreckenberg and A. Bachem (Eds.), *Traffic and Granular Flow*, World Scientific, Singapore, 1996.
[32] Z. Xiaoping, Z. Tingkuan and L. Mengting, Modeling crowd evacuation of a building based on seven methodological approaches, *Building and Environment*, **44** (2009), 437–445.

Received July 2017; revised November 2017.

E-mail address: ybg@bitp.kiev.ua
E-mail address: c.marschler@googlemail.com
E-mail address: mpso@dtu.dk
E-mail address: plch@dtu.dk
E-mail address: jjra@fysik.dtu.dk
E-mail address: jens.starke@uni-rostock.de